Insight into the role of copper in the promoted photocatalytic removal of NO using $Zn_{2-x}Cu_xCr\text{-}CO_3$ layered double hydroxide

J. Fragoso, M.A. Oliva, L. Camacho, M. Cruz-Yusta, G. de Miguel, F. Martin, A. Pastor, I. Pavlovic, L. Sánchez

PII: S0045-6535(21)00499-9

DOI: https://doi.org/10.1016/j.chemosphere.2021.130030

Reference: CHEM 130030

To appear in: *ECSN*

Received Date: 12 October 2020

Revised Date: 16 February 2021

Accepted Date: 17 February 2021

Please cite this article as: Fragoso, J., Oliva, M.A., Camacho, L., Cruz-Yusta, M., de Miguel, G., Martin, F., Pastor, A., Pavlovic, I., Sánchez, L., Insight into the role of copper in the promoted photocatalytic removal of NO using $Zn_{2-x}Cu_xCr\text{-}CO_3$ layered double hydroxide, *Chemosphere*, https://doi.org/10.1016/j.chemosphere.2021.130030.

J. Fragoso: Methodology, Investigation and Editing, M.A. Oliva: Investigation, L. Camacho: Software, Investigation and Writing, M. Cruz-Yusta: Investigation and Reviewing, G. de Miguel: Investigation, Writing and Reviewing, F. Martin: Investigation, Writing and Reviewing, A. Pastor: Investigation, I. Pavlovic: Methodology, Writing, Reviewing, L. Sánchez: Methodology, Writing - Original draft preparation, Reviewing and Editing

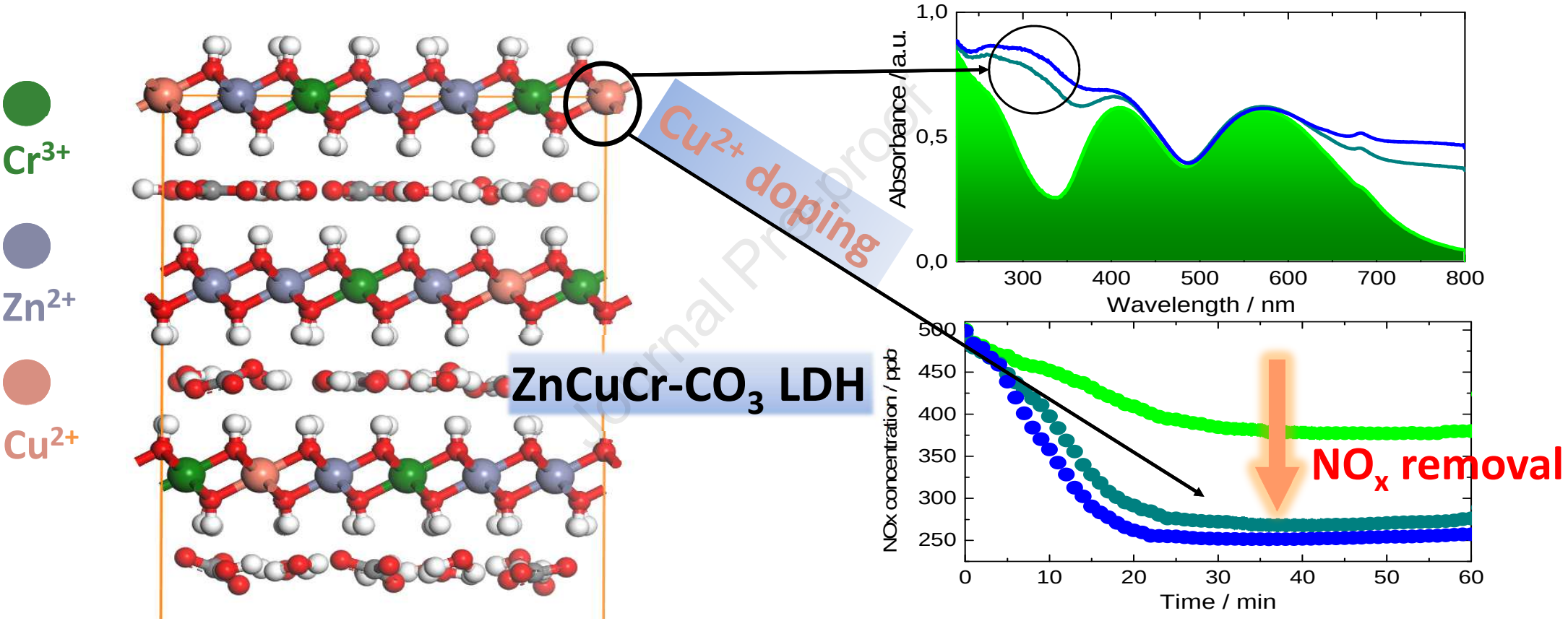

Insight into the role of copper in the promoted photocatalytic removal of NO using $Zn_{2-x}Cu_xCr\text{-}CO_3$ layered double hydroxide

J. Fragoso [1], M.A. Oliva [1], L. Camacho [2], M. Cruz-Yusta [1], G. de Miguel [2], F. Martin [3], A. Pastor[1], I. Pavlovic [1,]* and L. Sánchez [1,]*

[1] Departamento de Química Inorgánica e Ingeniería Química, Instituto Universitario de Nanoquímica IUNAN, Universidad de Córdoba, Campus de Rabanales, E-14014 Córdoba, España.

[2] Departamento de Química Física y Termodinámica Aplicada, Instituto Universitario de Nanoquímica IUNAN, Universidad de Córdoba, Campus de Rabanales, E-14014 Córdoba, España.

[3] Departamento de Ingeniería Química, Facultad de Ciencias, Universidad de Málaga, Campus de Teatinos, E-29071 Málaga, España.

* Corresponding Authors:

- Prof. Ivana Pavlovic

  ORCID ID: 0000-0003-2165-2940

  E-mail: pauli@uco.es

  Tel: +00-34-957-218648

- Prof. Luis Sánchez

  ORCID ID: 0000-0002-0194-1908

  E-mail: luis-sanchez@uco.es

  Tel: +00-34-957-218634

ABSTRACT

In this work the ability of $Zn_{2-x}Cu_xCr\text{-}CO_3$ layered double hydroxides (LDHs) as highly efficient DeNOx photocatalysts was studied. LDHs with x = 0, 0.2 and 0.4 were prepared using a coprecipitation method. The samples were characterized by different techniques such as XRD, XPS, FT-IR, ICP-MS, TG, SBET, SEM and Diffuse reflectance (DR). The increased amount of copper ions in the LDH layers gave rise to slight changes in the structure and morphology and an important variation of the optical properties of the LDHs. The prepared $ZnCuCr\text{-}CO_3$ photocatalysts exhibited favourable conversion efficiency (51 %) and an extraordinary selectivity (97 %) for the photochemical NO abatement. The photochemical mechanism was elucidated from DOS, EPR, Femtosecond transient absorption and in-situ DRIFTS studies. The results suggested that the presence of Cu^{2+} ions in the LDH framework introduced new states in the valence band states, thus favouring the production and mobility of e^-/h^+ charge carriers and a greater production of $\cdot O_2^-$ and $\cdot OH$.

KEYWORDS: LDH, Hydrotalcite, Photocatalysis, NO, in-situ DRIFTS

1. Introduction

NOx gases (NOx = NO + NO_2) are one of the priority pollutants in urban environments (European Environment Agency, 2017; Rodriguez-Rivas et al., 2018). There is a great interest for their remediation, since they produce highly toxic effects on human health and are related with thousands of early deaths (Borken-Kleefeld, 2017; Chen et al., 2004). From the early 2000s the use of photocatalysis has been successfully proved to remove NOx gases (DeNOx action) by using TiO_2 based materials (Angelo et al., 2013). However, some disadvantages are associated with the use of titania. Due to its large energy band gap (3.2 eV; $\lambda < 387$ nm) it can only capture solar energy efficiently in the ultraviolet region of sunlight. Additionally, photocatalytic titania is expensive as a raw material for large-scale applications in urban infrastructures. On the other hand, titania exhibits a low DeNOx selectivity, i.e. considerable emissions of NO_2 occur during the PCO process (Balbuena et al., 2015). These emissions should be avoided because the NO2 is more toxic than NO (Lewis, 2012). Additionally, the inhalation of TiO2 nanoparticles has recently been proposed as a cause of cancer (European Chemicals Agency, 2017). Therefore, there are scientific efforts on the study of new semiconductors such as modified titania (Balbuena et al., 2018b; Kim et al., 2019) or alternative compounds(Balbuena et al., 2018a; Chen et al., 2020; Hu et al., 2018; Huang et al., 2018; Pastor et al., 2019; Shen et al., 2021; Wang et al., 2020; Wu et al., 2020; Xiao et al., 2018), in order to find low cost, sustainable and enhanced DeNOx photocatalysts.

Layered double hydroxides (LDHs) have been proposed recently as efficient photocatalysts in environmental remediation processes (Fan et al., 2014; Mohapatra and Parida, 2016; Xiang et al., 2014). The LDH formula is represented as $[M^{2+}_{1-x}M^{3+}_{x}(OH)_2]^{x+}A^{n-}_{x/n}\cdot mH_2O$, where M^{2+} and M^{3+} are divalent and trivalent metal cations and A is the anion placed in the LDH interlayer (Cavani et al., 1991). The identity of the metals and anions, the M^{2+}/M^{3+} ratio or the co-existence of

multiple metals in the same framework have an influence on their electrical properties, and therefore on the absorption of light . The MO_6 octahedron in the layer is one of the key factors affecting the photocatalytic properties of LDHs. Through placing different metals at diverse ratios in the MO_6 octahedron, the energy band structure of the LDH is modified and should provide a better electron transfer, a lessened electron/hole recombination and improve sunlight harvesting (Tang et al., 2004; Wang et al., 2004). These reasons support the widespread use of these compounds as photocatalysts (Gomes Silva et al., 2009; Parida and Mohapatra, 2012; Shao et al., 2011; Wang et al., 2017; Yang et al., 2019).

Our research group has recently successfully proposed the use of LDH compounds as new low-cost DeNOx photocatalysts (vgr. LDH benchmark product is about 25 times cheaper than photocatalytic TiO_2), with successful results (Pastor et al., 2020; Rodriguez-Rivas et al., 2020, 2018). Because of the importance of the M-O octahedron connectivity in the LDH framework and its relationship with the energy band structure and charge transfer pathways, we explore for the first time in this work a ternary LDH constituted only of transition metals as DeNOx photocatalyst. For this purpose, we have based the study on the ZnCr-CO_3 LDH system, which has proved to be an efficient visible light photocatalyst (Gomes Silva et al., 2009; Parida and Mohapatra, 2012). The ternary system is obtained by doping with copper ion, a dopant successfully studied in ZnAl and ZnGa LDH photocatalysts (Ahmed et al., 2011; S. Kim et al., 2017). Thus, by formulating a $Zn_{2-x}Cu_xCr$-CO_3 LDH the full range of visible light is harvested (due to the presence of both Cu^{2+} and Cr^{3+}) and the low M^{2+}/M^{3+} ratio (2:1) favors the contact between the octahedron of different metals enhancing the charge transfer pathways. The samples will be fully characterized and the changes observed in their structural, morphological and optical properties commented on with relation to the enhanced DeNOx photocatalytic behaviour. In addition, the photochemical oxidation mechanism will be explained based on the

results obtained by using EPR, femtosecond transient absorption and in-situ DRIFT techniques and the estimated theoretical energy band structure, all of them highlighting the role of Cu^{2+} ion in the promoted photo-activity.

Experimental

2.1. Synthesis of LDHs

ZnCr and ZnCuCr LDHs were obtained by the co-precipitation method, with M^{2+}/M^{3+} = 2 and $Cu^{2+}/(Cu^{2+}+ Zn^{2+})$= 0, 0.1 and 0.2. A 1.5 M solution of $Zn(NO_3)_2{\cdot}6H_2O$, $Cu(NO_3)_2{\cdot}3H_2O$ and $Cr(NO_3)_3{\cdot}9H_2O$ with the appropriate metal ratio was added dropwise into 100 mL of 1M Na_2CO_3 solution under stirring at room temperature and pH = 10.0 ± 0.2. The resulting suspension was centrifuged and washed with distilled water (until there was no presence of nitrate impurities) and dried at 60 °C.

2.2. LDH characterization

X-ray diffraction (XRD) patterns of the samples were recorded by a Bruker D8 Discovery diffractometer. Thermogravimetric analysis (TGA) was performed on a TGA/DSC 1 Star System Mettler Toledo equipment in oxygen atmosphere (flow: 100 mL min^{-1}; heating rate: 5 °C·min^{-1}). Elemental chemical analyses were measured by induced coupled plasma mass spectroscopy (ICP-MS) on a Perkin Elmer Nexion-X instrument. The Fourier transform infrared spectrum (FT-IR) was recorded with Perkin-Elmer Frontier MIR using ATR. The scanning electron microscopy (SEM) morphological images were performed on a Jeol JSM 7800F microscope. Pore microstructure and textural properties were studied by N_2 adsorption-desorption isotherms on a Micromeritics ASAP 2020 apparatus. UV-Vis spectra were measured employing a Cary 5000

spectrophotometer. XPS was carried out with a Versaprobe II equipment from PHI provided with a focused monochromatic X-ray source (Al-Kα 1486.6 eV) with scanning and imaging capabilities.

Periodic Density of Functional Theory (DFT) calculations were carried out in order to build up the ZnCr and ZnCuCr LDHs and to calculate the density of states (DOS) plots of both structures.

2.3. Evaluation of the photocatalytic activity

The photocatalytic activity was investigated by examining the removal ratio of NO at ppb levels (500 ppb) in a continuous-flow reactor illuminated using a sunlight irradiation box.

In order to know about the participation of radical and chemical species in the photocatalytic process, the corresponding electron paramagnetic resonance (EPR) spectra, Femtosecond transient absorption measurements (S.-Y. Kim et al., 2017) and in situ diffuse reflectance infrared Fourier transform spectroscopy (DRIFTS) measurements were performed.

3. Results and Discussion

3.1 Characterization of LDH materials

The preparation of the ZnCr and ZnCuCr LDH samples was carried out following the previously reported experimental procedure (Rodriguez-Rivas et al., 2018). Following this procedure, all LDHs precipitated as very poor crystallized samples which, in any case is typical for LDH frameworks containing Cr^{3+} ions (Rodriguez-Rivas et al., 2020), as suggested by the broad and the low intensity diffraction peaks observed in Fig. 1a. The basal spacing (d_{003}) around 7.69 Å obtained for the $Zn_{2-x}Cu_xCr$ samples is in accordance with the presence of carbonate in the interlayer space (Baliarsingh et al., 2013). Even though the crystallinity was poor, it was observed

that the d_{003} reflection appeared slightly broader and shifted towards higher two-tetha angles in the case of the copper containing samples (Supporting Information; Fig. S1). The broadening is probably associated with a decrease in the size of the particles while the shifting of d_{003} reflections in the ZnCuCr-LDH samples could be due to the differences in the hydration state (S. Kim et al., 2017). Notwithstanding, slightly lower c values (Table 1), observed for Cu-bearing LDH samples, could be related to the incompatibility of copper to fit well in a regular octahedral network of LDH (Jan-Teller effect). In ZnCuCr-LDH samples, a disordered cation distribution could take place, thus provoking stacking faults and a flattering of the brucite-like layers along the c-axis.

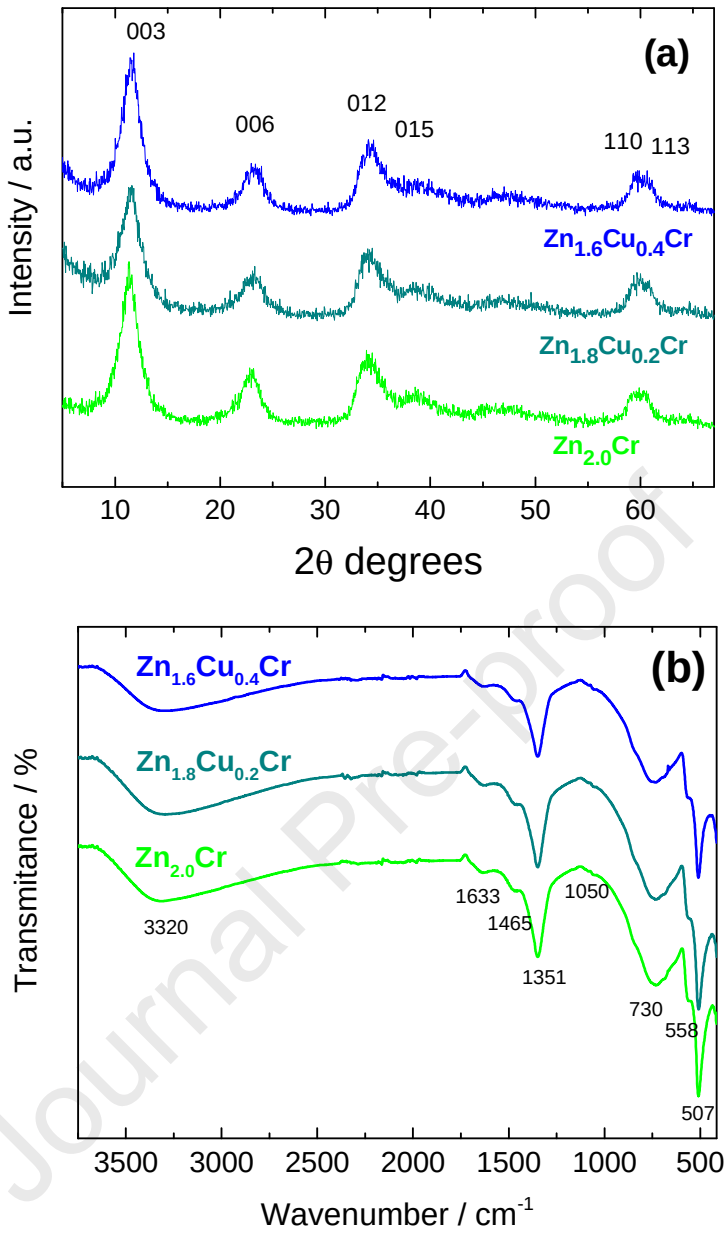

Figure 1. (a) XRD patterns and (b) IR spectra obtained from the ZnCr-LDH and ZnCuCr-LDH samples.

The chemical analysis (Table 1) confirmed that the M^{2+}/M^{3+} molar ratio in all the LDH samples was close to that in the starting solutions, i.e. M^{2+}/M^{3+} = 2. The corresponding thermogravimetric patterns (Fig. S2) served to calculate the amount of water molecules per formula. The carbonate content was that assumed necessary to compensate the excess of

positive charge originated by the presence of Cr^{3+} in a brucite type structure. On the other hand, XPS studies indicated the presence of Zn^{2+}, Cr^{3+} and Cu^{2+} species (Fig. S3).

Table 1. Physicochemical characterization for the LDH samples.

Sample	Atomic ratio		Proposed Formula	Lattice parameters	
	Cu^{2+}/M^{2+}	M^{2+}/M^{3+}		*a* (Å)	*c*(Å)
Zn_2Cr	--	2.13	$[Zn_{0.68}Cr_{0.32}(OH)_2](CO_3)_{0.16}\,0.37H_2O$	3.09	23.39
$Zn_{1.8}Cu_{0.2}Cr$	0.10	2.20	$[Zn_{0.62}Cu_{0.07}Cr_{0.31}(OH)_2](CO_3)_{0.155}\,0.58H_2O$	3.08	23.09
$Zn_{1.6}Cu_{0.4}Cr$	0.20	2.23	$[Zn_{0.55}Cu_{0.14}Cr_{0.31}(OH)_2](CO_3)_{0.155}\,0.60H_2O$	3.08	22.97

Fig. 1b shows FT-IR spectra for the ZnCr and ZnCuCr LDHs. The bands observed are those expected for pure LDH phases. The presence of O–H bonds is revealed by the broad band located at 3320 cm^{-1} and the H_2O bending vibration occurs at 1633 cm^{-1}, while bands observed at 1465 and 1351 cm^{-1} (the strongest band) correspond to the split asymmetric stretching mode of carbonate interlayer anions. Moreover, and as a result of this lowering symmetry of the interlayer carbonate, the IR inactive ν_1 vibration is activated, as a very weak almost imperceptible band at ~ 1050 cm^{-1} (Cavani et al., 1991). Concerning the basal layer, the OH–M–OH vibrational bending mode appears at 730 cm^{-1} and those for M–O at 558 and 507 cm^{-1}, which slightly shifts towards higher wavenumbers as Zn^{2+} is substituted by Cu^{2+} (S. Kim et al., 2017). The clear absence of a characteristic sharp nitrate peak at around 1380 cm^{-1} (Perez et al., 2012), permit us to conclude that the samples were well washed and free of eventual nitrate impurities from the metal precursors.

As mentioned above, and in according to the synthetic procedure, all samples were collected as poor crystallized compounds, Fig. 2. The SEM images of the Zn_2Cr sample show agglomerates of unshaped nanoparticles coexisting with a honeycomb nanometric lamellar macrostructure. Although the formation of lamellar structures is characteristic of LDH compounds, this is restricted on these samples because of the acidic character Cr^{3+} (Rodriguez-

205 Rivas et al., 2020). In samples containing copper, this lamellar macrostructure is minor and
206 practically evanished with an increase of the amount of copper, as in the case of the $Zn_{1.6}Cu_{0.4}Cr$
207 sample. Additionally, composition and microstructure was corroborated by TEM/HRTEM
208 observations, Fig. S4.

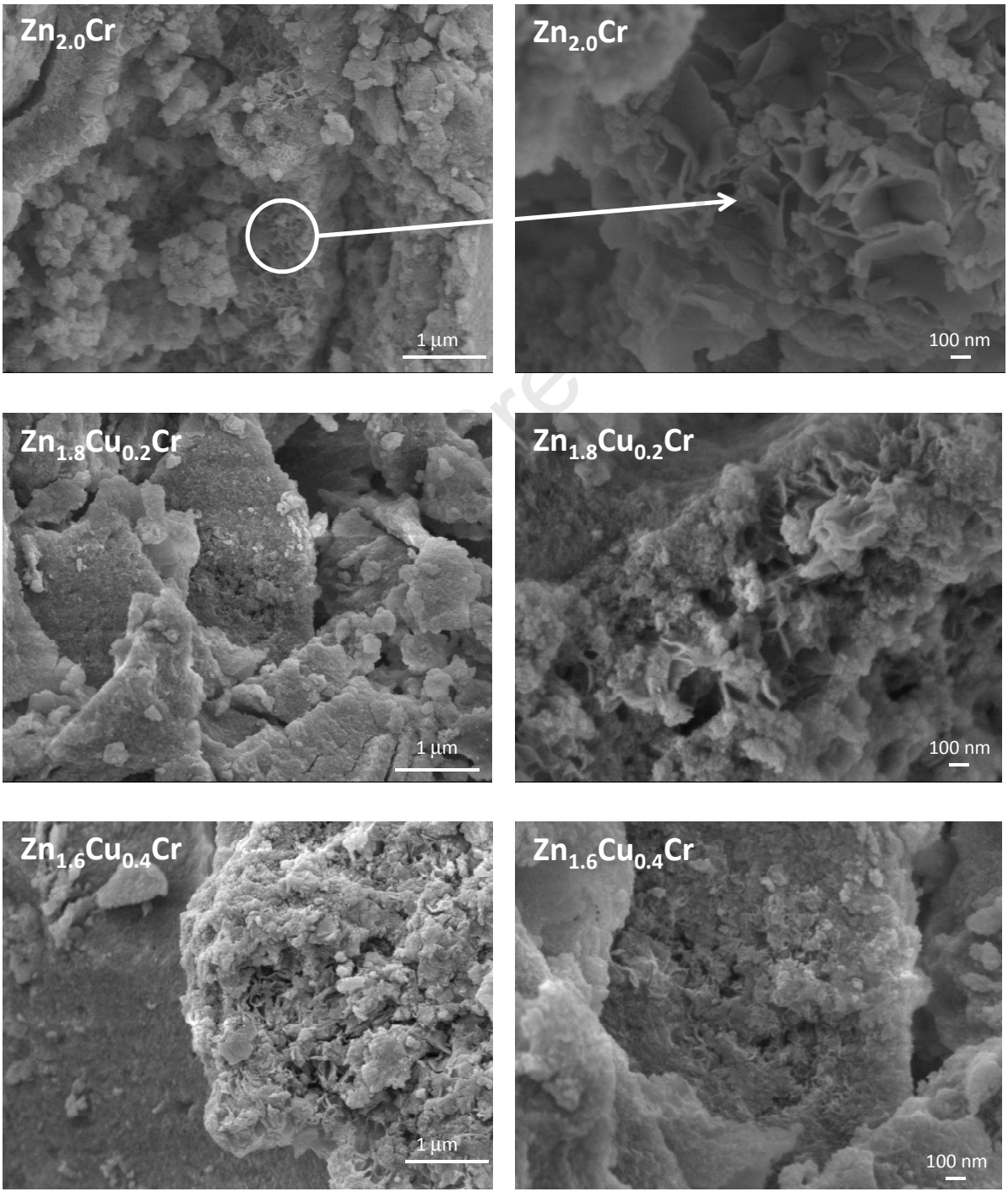

209

210 **Figure 2.** SEM images of the ZnCr-LDH and ZnCuCr-LDH samples.

The pore microstructure of each sample was analysed from the corresponding N_2 adsorption-desorption isotherms, Fig. S5. The specific surface area values measured by BET method were 94, 100 and 140 $m^2 \cdot g^{-1}$ for Zn_2Cr, $Zn_{1.8}Cu_{0.2}Cr$ and $Zn_{1.6}Cu_{0.4}Cr$ samples, respectively. These increased values observed when the copper content increased in the LDH are concordant with the decrease of the crystallinity shown in XRD patterns (Fig. 1) and SEM images (Fig. 2).

The presence of Cu^{2+} in the LDH framework allows for improved harvesting of the UV-Vis light, and doped samples showed new absorption bands at 300 and 785 nm which were not observed for the Zn_2Cr sample, Fig. S6.

3.2 Photocatalytic DeNOx tests

The photocatalytic activity of the samples studied was evaluated considering their potential to eliminate nitrogen oxides from air through a photochemical oxidation process (PCO), following the experimental procedure described in SI. In Fig. 3a, the variation on the NO, NO_2 and NO_X concentration measured during a standard test for the Zn_2Cr photocatalyst is represented. During the first 15 minutes the NO concentration measured is nearly constant, therefore there is no substantial interaction between the inlet NO gas and the catalyst or chamber. When the light is on, a fast decay of the NO concentration is observed indicating that NO is being transformed by a light activated chemical process. In fact, once the light is off the NO concentration returns to the initial values. The following summarized sequential steps are assumed for the $DeNO_X$ test: $NO \rightarrow HNO_2 \rightarrow NO_2 \rightarrow NO_3^-$.

This oxidative mechanism accounts for the presence of high reactive oxygen species (ROS). Once the LDH photocatalyst is irradiated with the appropriate light, the photon energy is briefly transferred to the electron (e^-) in the valence band (VB), which jumps to the conduction band

(CB), leaving a hole (h^+) in VB. When both mobile charges reach the surface of the catalyst particles, then water and oxygen adsorbed molecules suffer redox reactions producing ·OH and $\cdot O_2^-$ radicals (ROS species), which initiate and participate in the oxidation of nitrogen oxide gases (Balbuena et al., 2015). In the case of the sequential reaction being completely selective, all the NO would be oxidised to nitrate. However, the production of intermediates like NO_2 gas are frequently detected (Balbuena et al., 2018a). This intermediate must be avoided because it is highly more toxic compared to NO_2 (Bloh et al., 2014). In the case of our samples, serving as a representative of the concentration profiles of Fig. 3a, the release of NO_2 is negligible and reduced to a few ppb (3-5 ppb). Therefore, the DeNOx selectivity exhibited by these LDHs is outstanding with values > 97 %. It is worth mentioning that such high selectivity values are difficult to attain only being reported for some DeNOx advanced photocatalysts (Balbuena et al., 2018b; Leinen et al., 2019; Pastor et al., 2020, 2019; Shang et al., 2019; Tan et al., 2017). Finally, the whole removal of nitrogen gases from the air is considered following the NOx concentration profile (Fig. 3a), taking into account the sum of NO and NO_2 concentrations. When this NOx profile is compared from the three samples (Fig. 3b), it is observed that the slope of the initial concentration decay is higher as the copper content increases in the LDH sample, indicating that the photocatalytic activity is favoured in the copper-based systems. In fact, the initial rate constants for NOx degradation are higher in these samples (Fig. S7).

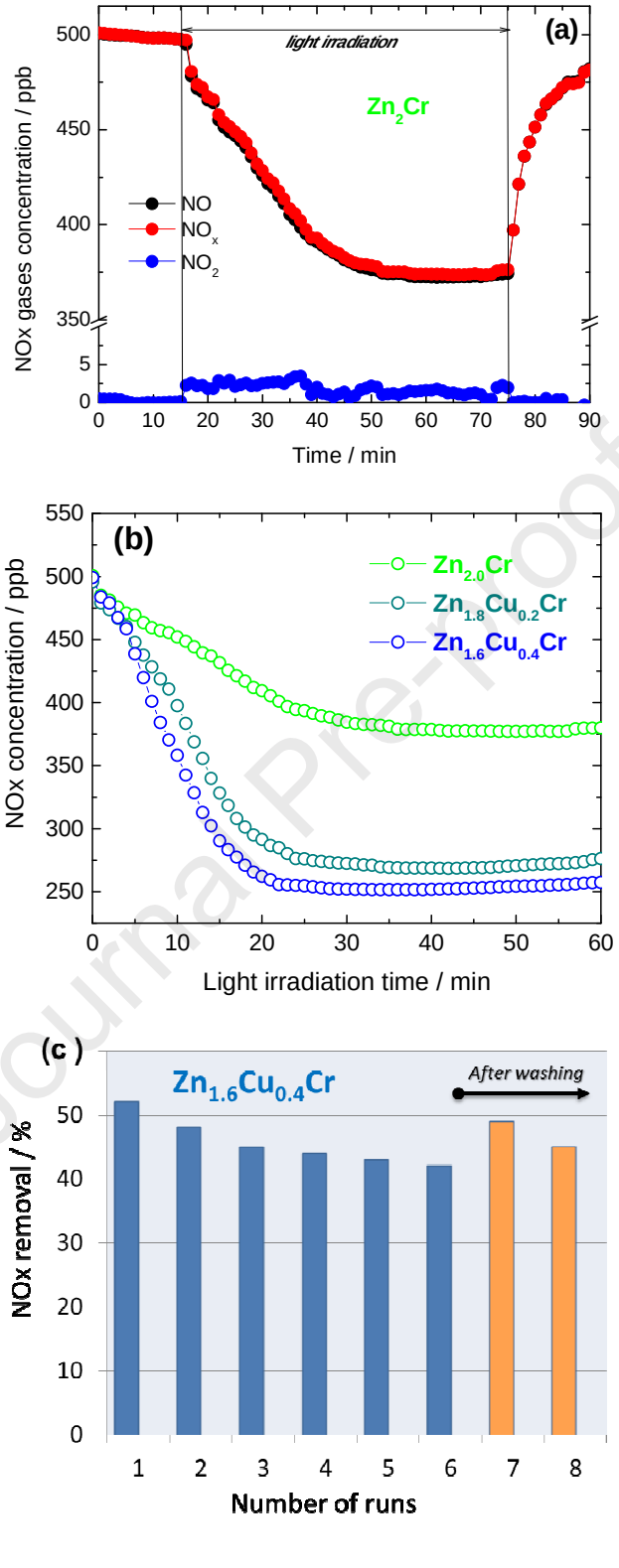

Figure 3. (a) NO, NO_2 and NOx gases concentration evolution during the photo-degradation of gaseous NO under UV–Vis light irradiation on the Zn_2Cr sample. (b) Photo-oxidative removal of NOx gas concentration measured under UV–Vis light irradiation on ZnCr-LDH and ZnCuCr-LDH catalysts. (c) NO removal efficiency calculated for each run of the reusability tests for the $Zn_{1.6}Cu_{0.4}Cr$ sample.

Once the steady state is reached after the first 20 minutes of sunlight irradiation, the efficiency in the NOx removal is also higher for samples containing copper, the values being estimated at 27 %, 45 % and 51 % for Zn_2Cr, $Zn_{1.8}Cu_{0.2}Cr$ and $Zn_{1.6}Cu_{0.4}Cr$ samples, respectively. There is a clear correlation between the increase in the DeNOx efficiency and the amount of Cu in the LDH formulation. Conversely, considering that Zn_2Cr and $Zn_{1.8}Cu_{0.2}Cr$ samples possess similar specific surface areas, the presence of copper as a doping element in the ZnCr-LDH framework seems to be of key importance in explaining the enhanced photocatalytic activity observed. In fact the $Zn_{1.8}Cu_{0.2}Cr$ LDH DeNOx photocatalyst, with comparison to LDH photocatalysts previously studied by our research group (Pastor et al., 2020; Rodriguez-Rivas et al., 2020, 2018), surpass in ≈ 40 % the efficiency of NO removal showed by LDHs with similar M^{2+}/M^{3+} ratio (2:1) and exhibits the highest selectivity values (S > 97 %), evidencing the advantage to prepare a ternary LDH constituted only of transition metals. Regarding the reusability of the photocatalyst, several successive run tests were performed on the $Zn_{1.6}Cu_{0.4}Cr$ sample (Fig. 3c). For each test, the sample was irradiated for 1 h. The NOx efficiency slowly decays during the first 6 tests which is due to the accumulation of nitrite/nitrate species on the particle surface of the photocatalyst as will be proved here further on. These species are highly soluble and are eliminated when the sample is collected and washed with milli-Q water after the sixth run. In fact, in the following runs, number 7 and 8, the photocatalytic performance is recovered, which proves the reusability of ZnCuCr-LDH as a DeNOx photocatalyst.

Moreover, the photocatalytic activity under visible light was examined once the DeNOx test was carried out under $\lambda > 400$ nm light. In Fig. S8, it can be observed that the NO abatement is enhanced in the copper containing samples, which should be associated with better visible light harvesting.

3.3 Photocatalytic mechanism

The following experiments were performed in order to know the photocatalytic mechanism expected for the copper doped LDH photocatalyst. As was previously commented, the NO_X gases were removed following a PCO process assisted by the reactive oxygen species (ROS). In order to shed light on the reactive species involved when ZnCr and ZnCuCr LDHs were used as photocatalysts, EPR measurements were performed using DMPO as the spin-trapping agent under sunlight excitation, Figs. 5a and 5b. In the absence of light irradiation, no signal was detected for the photocatalyst suspension (blank). In all the samples, the characteristic signal of DMPO-·OH adduct appears as a quartet of peaks featuring a 1:2:2:1 intensity ratio, Fig. 4a. In the case of the DMPO-·O_2^- signal, a sextet of peaks is observed for the three samples, Fig. 4b, in similitude to those previously registered for Zn based LDH compounds (Huang et al., 2018; Pastor et al., 2020; Rodriguez-Rivas et al., 2020; Yang et al., 2017). The intensity of both signals increases with the Cu content, which is remarkable in the case of the $\cdot O_2^-$ signal. Therefore, the Cu^{2+} doping clearly enhances the ability to generate active radicals. These results confirm that ROS radical species, mainly $\cdot O_2^-$, are involved in the NO photochemical oxidation accounted for ZnCuCr-LDH photocatalysts.

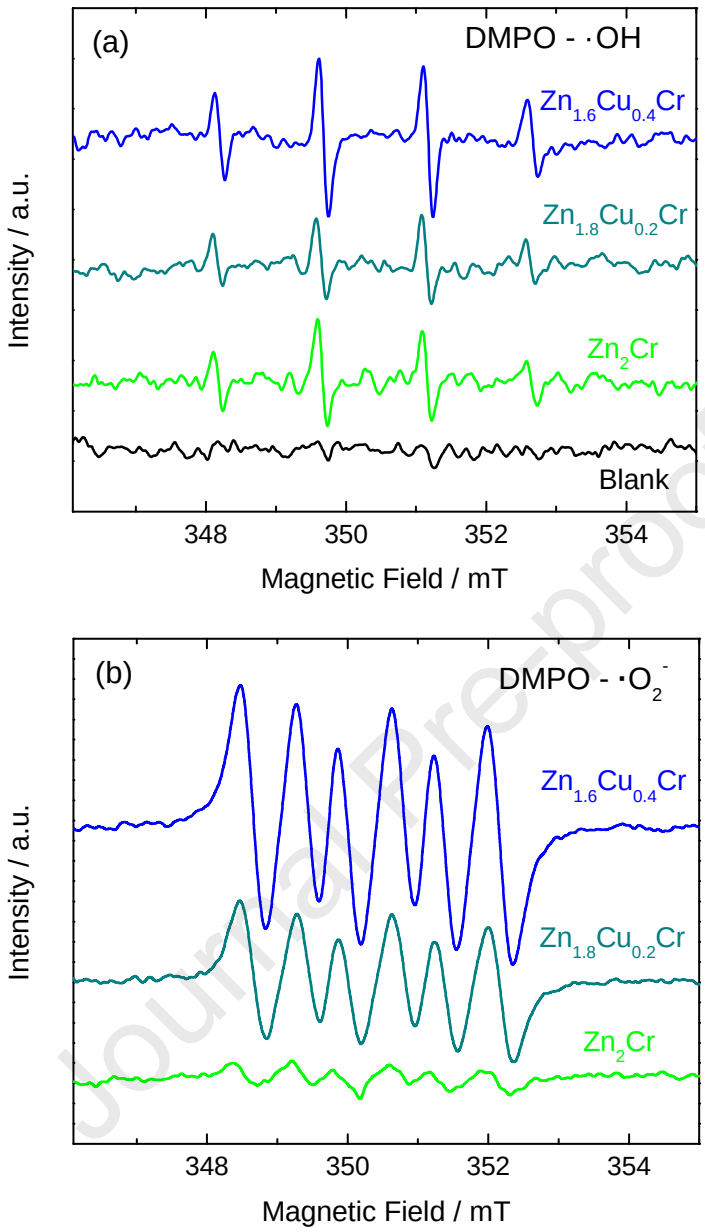

344

345 **Figure 4.** DMPO spin-trapping EPR spectra of the ZnCr-LDH and ZnCuCr-LDH samples under UV–
346 Vis light irradiation for 15 min in (a) aqueous solution for ·OH and (b) methanol solution
347 for $\cdot O_2^-$.

348

349 Theoretical calculations in order to investigate the atomic nature of the valence and
350 conduction bands were performed for the ZnCr and ZnCuCr LDHs. Fig. 5 displays the
351 $Zn_{36}Cr_{18}(OH)_{108}(CO_3)_9(H_2O)_{27}$ and $Zn_{29}Cu_7Cr_{18}(OH)_{108}(CO_3)_9(H_2O)_{27}$ supercells exhibiting the
352 layered structure of these materials and the sequential incorporation of Cu to the parent ZnCr

LDH. The density of states (DOS) diagrams calculated for the undoped and doped theoretical LDH structures highlight the role of copper ions. The DOS diagrams are calculated for both structures obtaining alpha and beta plots due to the presence of unpaired electrons in the Cr and Cu atoms. Fig. S9 depicts the total and partial (for each metal atom) DOS plots for Zn_2Cr LDH in the alpha and beta states. The total DOS diagram displays a band gap of about 1 eV, slightly lower compared to the 1.5 eV, experimentally measured in the absorption measurements. The *d* orbitals are mostly responsible for both valence and conduction bands with a small contribution of the *p* orbitals in the alpha states. However, the most remarkable feature is revealed in the partial DOS plots, where only the *d* orbitals of the Cr atoms are responsible for the valence and conduction bands with the *d* orbitals of the Zn atoms deeply buried at low energies in the valence band. These results agree favourably with those previously reported in the literature (Xu et al., 2017). Regarding the $Zn_{1.6}Cu_{0.4}Cr$ LDH, Fig. 6, the DOS plots display similar behavior to that of Zn_2Cr LDH with the *d* orbitals contributing mostly to the valence and conduction bands. However, the partial DOS diagrams show that the *d* orbitals from the Cu atoms contribute significantly to the valence band without participating in the conduction band. Thus, the new electronic states due to Cu orbitals in the valence band of the ZnCuCr LDHs may involve the appearance of novel absorption bands, as has been experimentally observed with the appearance of new peaks at 300 nm and 785 nm in the absorption measurements. The photoexcitation of the Cu-based states in the valence band of the ZnCuCr LDHs involves the formation of energetic holes that might participate in the photocatalytic reactions, unlike the situation of the ZnCr LDHs, which favours the formation of ROS species as inferred from the EPR measurements (Fig. 4).

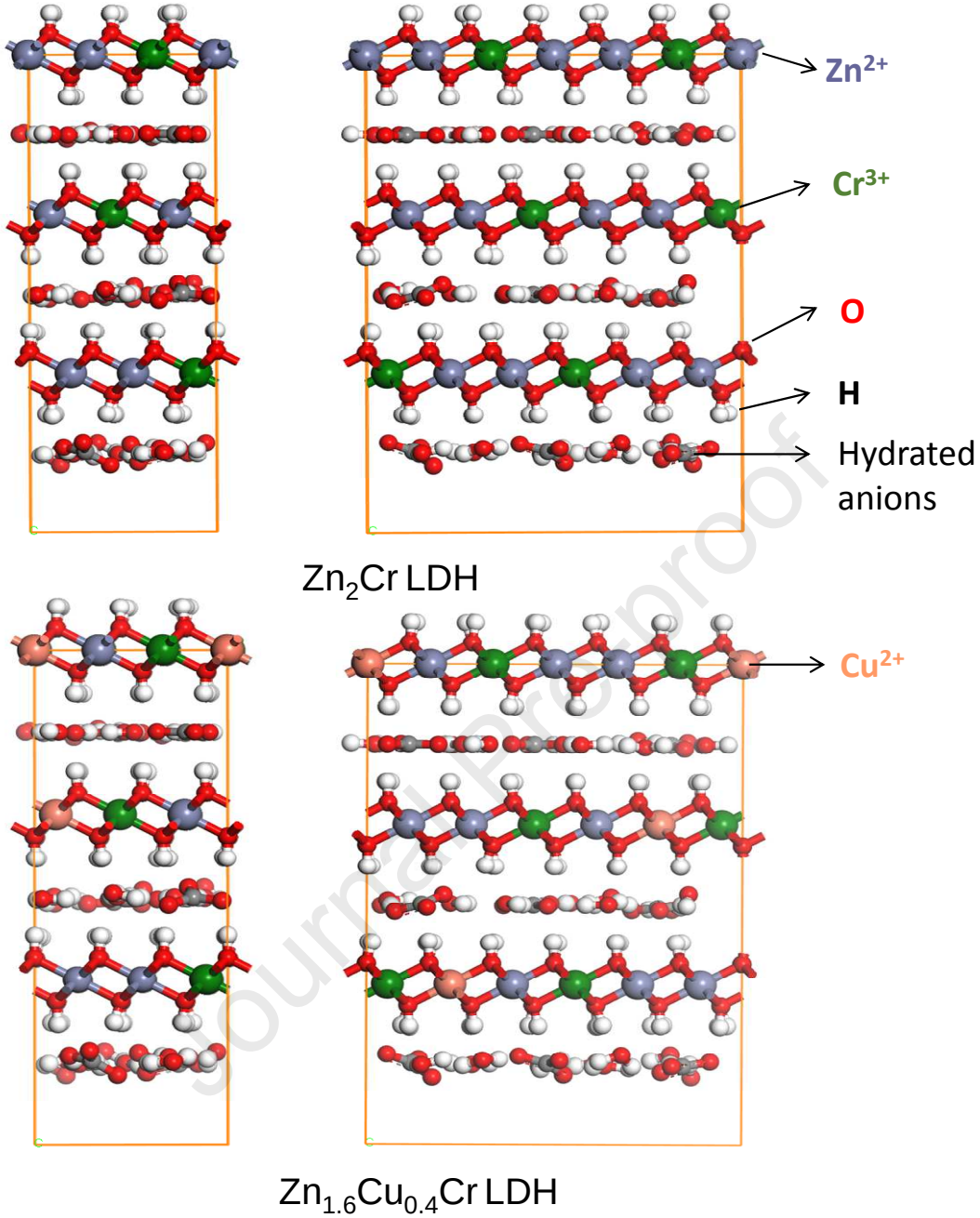

375

376 **Figure 5.** Schematic representation of the structure of, $Zn_{36}Cr_{18}(OH)_{108}(CO_3)_9(H_2O)_{27}$ and
377 $Zn_{27}Cu_9Cr_{18}(OH)_{108}(CO_3)_9(H_2O)_{27}$ LDHs supercells, side and front view of the layer.

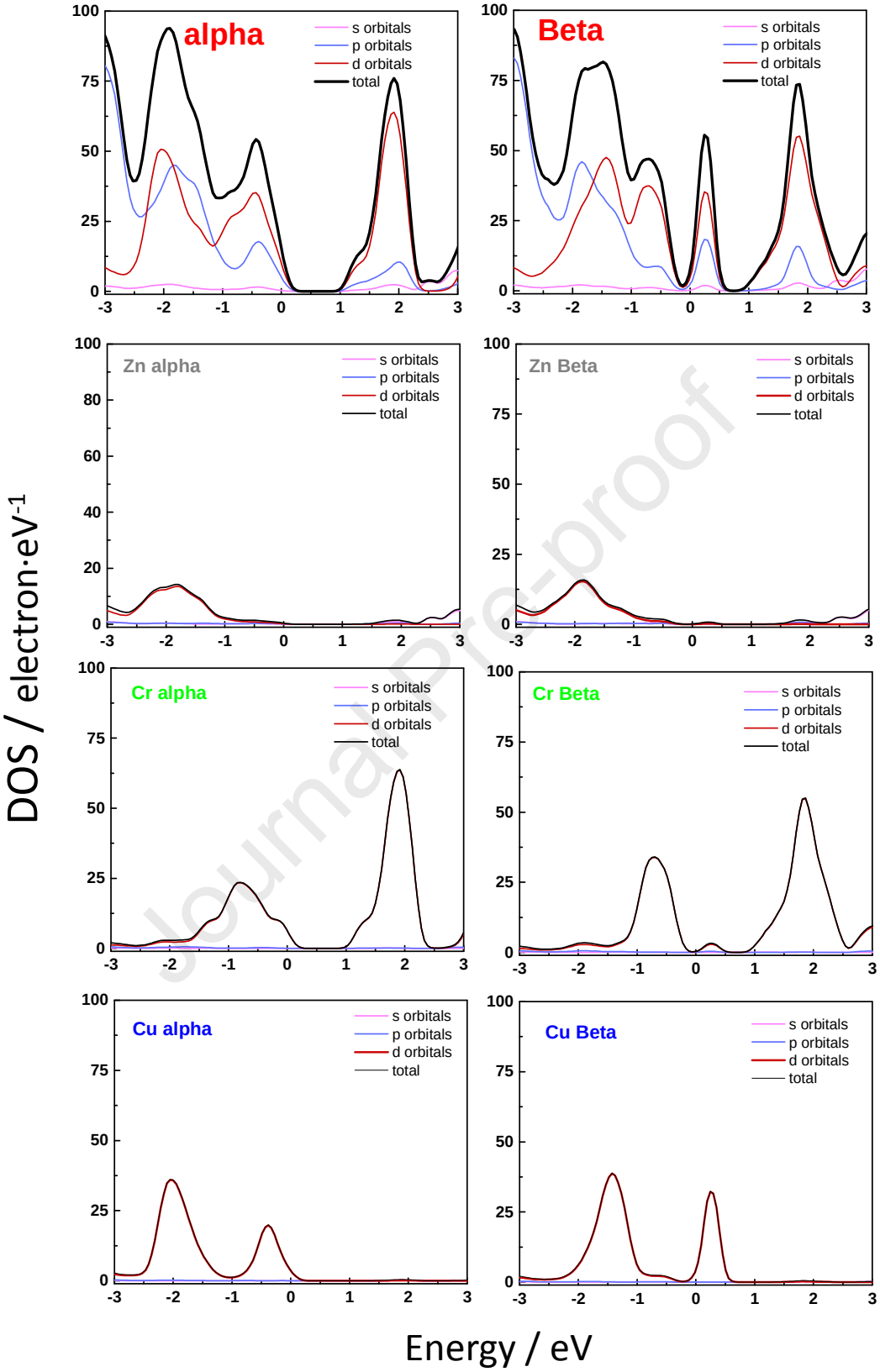

378

379 **Figure 6.** Calculated total density of states (DOS) and projected density of states (PDOS) of the
380 Zn, Cu and Cr atoms in the alpha and beta states of the $Zn_{1.6}Cu_{0.4}Cr$ photocatalyst.

To investigate the formation of new electronic states in the ZnCuCr LDHs, femtosecond transient absorption measurements were performed in both photocatalysts. Fig. S10 displays the transient spectra of the Zn_2Cr (A) and $Zn_{1.6}Cu_{0.4}Cr$ (B) LDHs after excitation at 300 nm. The broad positive signal with a maximum value around 480 nm is assigned to the photoinduced absorption (PIA) of the excited electrons in the conduction band. Both LDHs photocatalysts exhibit similar PIA signals which proves the formation of excited electrons with the same energy. Fig. S10 (C and D) depicts the time profiles at 480 nm with the best bi-exponential fits for both photocatalysts and with the signal not recovering completely after 4 ns. The deactivation kinetics for the excited state in both LDHs is developed in the same time range with time constant of 27 ns and 1170 ns for Zn_2Cr LDH and 73 ns and 2125 ns for $Zn_{1.6}Cu_{0.4}Cr$ LDH. Thus, the recombination kinetics of the electrons in the $Zn_{1.6}Cu_{0.4}Cr$ LDH was slightly slower, which might enhance the photocatalytic activity of this compound. Moreover, the superior performance of the ZnCuCr LDHs might also be attributed to an enhanced sunlight harvesting ability or the formation of energetic holes.

Subsequently, in situ DRIFTS measurements were carried out during the dynamic monitoring of the detailed mechanism involved in the photocatalytic removal of NO. Firstly, the samples were subjected to pretreatment and NO adsorption processes. The background spectrum was recorded before NO flow passed through the reaction chamber. Fig. 7a shows the spectra obtained in each sample, once the background had been subtracted, after 10 min of NO flow in dark conditions. Apart the new increased signals corresponding to the apparition of nitrogen oxide species, retrorse peaks were detected in the Zn_2Cr sample indicating that some pristine IR bands were decreasing. These are the peaks located at 1400-1350 and 1057 cm^{-1} mentioned above (Fig. 1b). This means that some slight perturbation occurred in the interlayer space under the NO flow. In fact, this is also reflected in the 3000 cm^{-1} region of the spectra (Fig. S11), where bands assigned to the interactions of hydrogen bonds between hydroxyl groups,

405 anions and water molecules, are registered (Rives, 2001). However, the structure of the doped
406 samples seems to be preserved during the NO flow. This difference could be associated with a
407 somewhat different position/symmetry of CO_3^{2-} in the LDH interlayers since ZnCr and ZnCuCr
408 LDHs exhibited different "*c*" crystallographic parameters. Regarding the newly appeared bands
409 assigned to nitrogen oxides species, differences were found between non-doped and Cu-doped
410 samples, Fig. 7a. Table S1 lists the assignment of the observed bands. In the case of ZnCuCr-LDH
411 samples, the NO molecules adsorbed in the surface are disproportionate in the presence of the
412 hydroxyl LDH groups, as NO^- (1353 cm^{-1}) and NO_2^- (828, 1330-1343, 1472 cm^{-1}) species appeared
413 (Liao et al., 2020). The rest of the bands are associated with the presence of NO_2, nitrite and
414 nitrates species.
415 The main transformations are considered as follows:
416
417 $2NO + OH^- \rightarrow HNO_2 + NO^-$ (1)
418 $NO + HNO_2 + OH^- \rightarrow NO^- + NO_2 + H_2O$ (2)
419 $NO^- + NO_2 \rightarrow NO_2^- + NO$ (3)
420 $NO^- + 2NO_2 \rightarrow NO_3^- + 2NO$ (4)
421

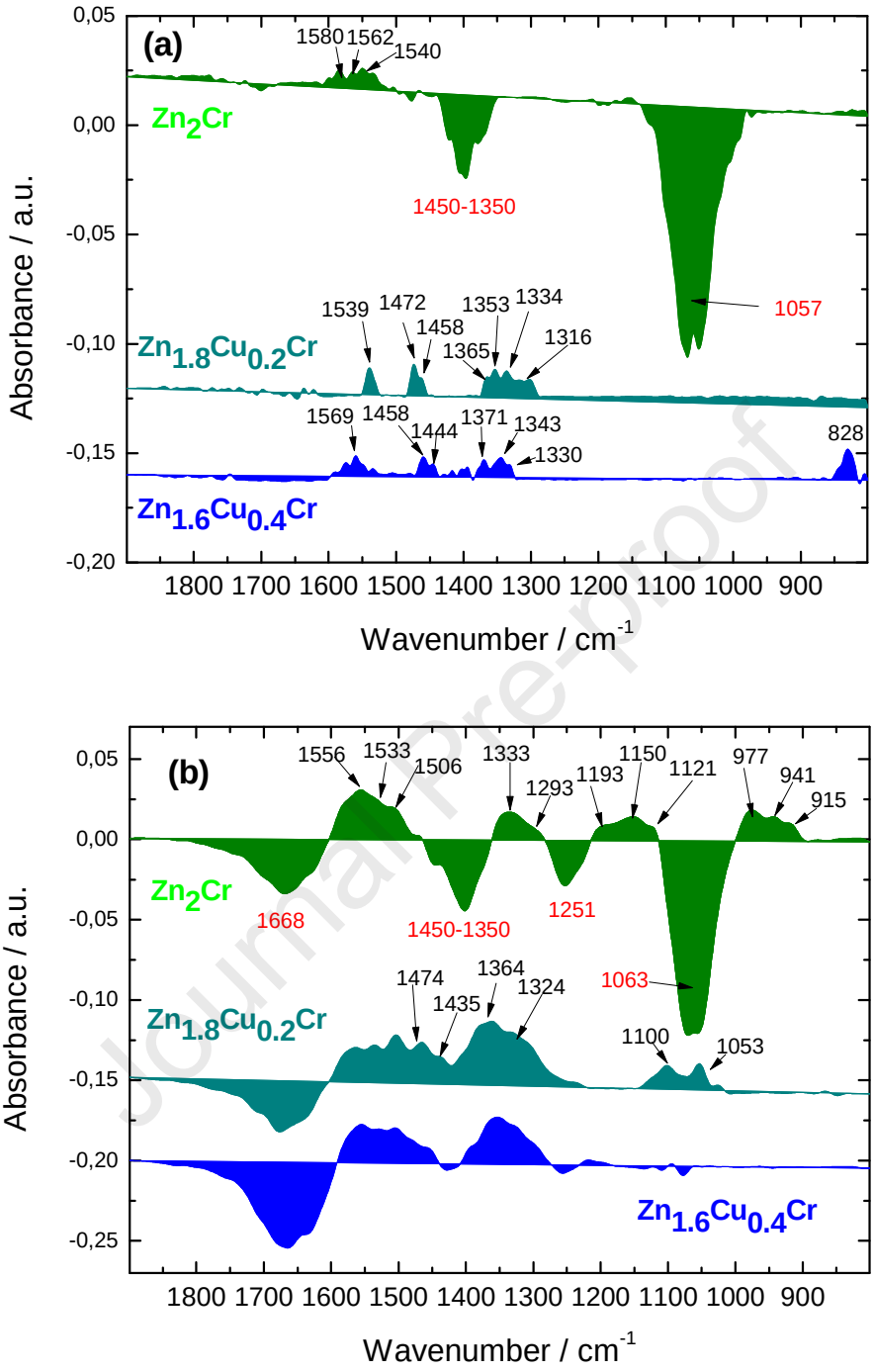

422

423 **Figure 7.** In situ DRIFTS spectra of NO adsorption (a) and oxidization processes under UV light
424 illumination (b) over ZnCr-LDH and ZnCuCr-LDH samples.
425
426
427

The above process is more difficult to elucidate in the case of the Zn_2Cr sample. Thus, the presence of a retrorse peak in the 1350-1440 cm^{-1} range could mask the presence of some bands corresponding to NO^-, NO_2^- and NO_2 species. On the other hand, there is some uncertainty in identifying the bands which appeared in the 1500-1600 as nitrate species. In fact, the presence of bicarbonate ion in LDHs has been identified at 1500-1550 cm^{-1} which is formed when a proton is transferred from the hydroxide sheet to the interlayer carbonate ion upon dehydration (Barriga et al., 1996; Clause et al., 1991). This matches with the findings associated with the retrorse peaks. In summary, the NO adsorption is favored in the copper doped samples, in accordance with the reported favorable absorption energy for the NO $\rightarrow$ Cu^{2+} binding (Mullen and Dutta, 2016).

Following the preliminary NO adsorption step, the oxidization process of NO under UV light irradiation was continuously monitored (Fig. S12). Fig. 7b shows the final products obtained on the surface of the photocatalysts after one hour of light irradiation. The new retrorse peak at 1668 cm^{-1} indicates that constituent water molecules play a role in the photocatalytic process, Equation (6). This signal is higher in the $Zn_{1.6}Cu_{0.4}Cr$ sample, in accordance with its higher ability to produce ·OH radicals, as inferred from the EPR measurements. No signals corresponding to NO_2 were observed in agreement with the high selectivity exhibited by these samples. This indicates that NO_2, if formed, is quickly oxidized to nitrate. In comparison with other $DeNO_X$ photocatalysts, the studied LDHs exhibit two characteristics facilitating this process: i) Zn based photocatalysts exhibit high sensitivity to NO_2 adsorption, remaining the gaseous molecules on surface for ulterior redox process (Pastor et al., 2020, 2019); ii) the participation of structural water molecules (OH^- groups) in the photocatalytic process enriches the formation of ROS species (Lv et al., 2020). Table S1 shows the multiple signals assigned to the following nitrogen oxide species: NO^-, NOH, NO_2^-, NO_3^-. These signals of oxidized species increase in intensity with

452 the increasing of illumination time, showing a tendency to form nitrites and nitrates as final
453 products (Fig. S12), corroborating the passivation of the photocatalyst´s surface observed during
454 the reusability test (Fig. 3c). The NO^- and NOH bands, in relation to the disproportionation of the
455 NO adsorbed molecule (Chen et al., 2020), are significantly present in the Zn_2Cr photocatalyst,
456 showing the lower ability of this photocatalyst to promote photo-activated processes, as was
457 observed from EPR studies. Considering the results obtained, in line with previous reports on
458 DeNOx photocatalysts (Huo et al., 2019b, 2019a), the primary NO oxidation reaction mechanism
459 can be described as follows:

460 $LDH + h\nu \rightarrow h^+ + e^-$ (5)

461 $h^+ + H_2O \rightarrow H^+ + \cdot OH$ (6)

462 $e^- + O_2 \rightarrow \cdot O_2^-$ (7)

463 $NO + \cdot O_2^- \rightarrow NO_2^-$ (8)

464 $NO + \cdot OH \rightarrow HNO_2$ (9)

465 $NO_2^- + \cdot OH \rightarrow HNO_3$ (10)

466 $HNO_2 + \cdot O_2^- \rightarrow HNO_3^-$ (11)

467 The in situ DRIFTS spectra evidence the higher efficiency of doped samples in promoting NO
468 photochemical oxidation, the nitrites and nitrates species being the final species obtained.

469

470 ## 4. Conclusions

471 $Zn_{2-x}Cu_xCr\text{-}CO_3$ LHDs (x = 0.2 and 0.4) photocatalysts were able to activate the photochemical
472 oxidation of NO molecules under UV-Vis and Vis light irradiation. All samples showed an
473 outstanding selectivity towards the NO photochemical process with values of S > 97 %.
474 Reusability was positively tested in the best of the photocatalysts.

The role of copper ions was highly significant in the promotion of the photochemical activity. Firstly, the presence of Cu^{2+} in the LDH framework allows for improved harvesting of the UV-Vis light. The DOS study reveals that increased amount of mobile e^-/h^+ charge carriers should be produced in ZnCuCr photocatalysts when they are light irradiated which is in agreement with the results obtained from the EPR studies, allows the formation of larger amounts of ·OH and $\cdot O_2^-$ radical species. On the other hand, the femtosecond transient absorption showed a slightly retarded electron-hole recombination. The in situ DRIFTS spectra evidence the higher efficiency of ZnCuCr samples in promoting NO photochemical oxidation.

Acknowledgements

This work was partly financed by the Junta de Andalucía (PAI Groups FQM-214 and FQM-175) and the Spanish Government (MAT2017-88284-P and CTQ2017-84221-R). Adrián Pastor and Javier Fragoso acknowledge a grant from the Spanish Government (FPU16/05041 and PRE2018-084594, respectively)

Supporting Information

Sample characterization. XRD and Thermogravimetric patterns, XPS and UV–Vis absorption spectra, TEM/HRTEM images, N_2 adsorption-desorption isotherms, Rate constants for NOx degradation, DeNOx values under Vis light irradiation; Calculated total density of states for the Zn2Cr LDH, Transient absorption spectra and in situ DRIFTS spectra.

References

Ahmed, N., Shibata, Y., Taniguchi, T., Izumi, Y., 2011. Photocatalytic conversion of carbon dioxide into methanol using zinc-copper-M(III) (M = aluminum, gallium) layered double hydroxides. J. Catal. 279, 123–135. https://doi.org/10.1016/j.jcat.2011.01.004

Angelo, J., Andrade, L., Madeira, L.M., Mendes, A., 2013. An overview of photocatalysis phenomena applied to NO_x abatement. J. Environ. Manage. 129, 522–539. https://doi.org/10.1016/j.jenvman.2013.08.006

Balbuena, J., Cruz-Yusta, M., Pastor, A., Sanchez, L., 2018a. α-Fe_2O_3/SiO_2 composites for the enhanced photocatalytic NO oxidation. J. Alloys Compd. 735, 1553–1561. https://doi.org/10.1016/j.jallcom.2017.11.259

Balbuena, J., Cruz-Yusta, M., Sánchez, L., 2015. Nanomaterials to Combat NO_x Pollution. J. Nanosci. Nanotechnol. 15, 6373–6385. https://doi.org/10.1166/jnn.2015.10871

Balbuena, J., Calatayud, J.M., Cruz-Yusta, M., Pardo, P., Martin, F., Alarcon, J., Sanchez, L., 2018b. Mesocrystalline anatase nanoparticles synthesized using a simple hydrothermal approach with enhanced light harvesting for gas-phase reactiont. Dalt. Trans. 47, 6590–6597. https://doi.org/10.1039/c8dt00721g

Baliarsingh, N., Mohapatra, L., Parida, K., 2013. Design and development of a visible light harvesting Ni-Zn/Cr-CO_3^{2-} LDH system for hydrogen evolution. J. Mater. Chem. A 1, 4236–4243. https://doi.org/10.1039/c2ta00933a

Barriga, C., Kooli, F., Rives, V., Ulibarri, M.A., 1996. Layered Hidroxycarbonates with the Hydrptalcite Structure Containing Zn, Al, and Fe, in: Occelli, M.L., Kessler, H. (Eds.), Synthesis of Porous Materials: Zeolites: Clays, and Nanostructures, Chemical Industries. Marcel Dekker, New York, pp. 661–674.

Bloh, J.Z., Folli, A., Macphee, D.E., 2014. Photocatalytic NO_x abatement: why the selectivity matters. RSC Adv. 4, 45726–45734. https://doi.org/10.1039/c4ra07916g

Borken-Kleefeld, J., 2017. International Institute for Applied Systems Analysis [WWW Document]. URL https://iiasa.ac.at/web/home/about/news/170918-diesel-nox.html (accessed 16 March 2020).

Cavani, F., Trifirò, F., Vaccari, A., 1991. Hydrotalcite-type anionic clays: Preparation, properties and applications. Catal. Today 11, 173–301. https://doi.org/https://doi.org/10.1016/0920-5861(91)80068-K

Chen, B.H., Hong, C.J., Kan, H.D., 2004. Exposures and health outcomes from outdoor air pollutants in China. Toxicology 198, 291–300. https://doi.org/10.1016/j.tox.2004.02.005

Chen, P., Liu, H., Sun, Y., Li, J., Cui, W., Wang, L., Zhang, W., Yuan, X., Wang, Z., Zhang, Y., Dong, F., 2020. Bi metal prevents the deactivation of oxygen vacancies in $Bi_2O_2CO_3$ for stable and efficient photocatalytic NO abatement. Appl. Catal. B Environ. 264. https://doi.org/10.1016/j.apcatb.2019.118545

536 Clause, O., Gazzano, M., Trifiro, F., Vaccari, A., Zatorski, L., 1991. Preparation and thermal
537 reactivity of nickel chromium and nickel aluminum hydrotalcite-type precursors. Appl. Catal.
538 73, 217–236. https://doi.org/10.1016/0166-9834(91)85138-L

539 European Chemicals Agency, 2017. Annex 2- Comments and response to comments on CLH
540 PROPOSAL on Titanium dioxide.

541 European Environment Agency, 2017. European Union emission inventory report 1990-2015
542 under the UNECE Convention on Long-range Transboundary Air Pollution (LRTAP).
543 Luxembourg. https://doi.org/10.2800/478321

544 Fan, G., Li, F., Evans, D.G., Duan, X., 2014. Catalytic applications of layered double hydroxides:
545 recent advances and perspectives. Chem. Soc. Rev. 43, 7040–7066.
546 https://doi.org/10.1039/C4CS00160E

547 Gomes Silva, C., Bouizi, Y., Fornes, V., Garcia, H., 2009. Layered Double Hydroxides as Highly
548 Efficient Photocatalysts for Visible Light Oxygen Generation from Water. J. Am. Chem. Soc.
549 131, 13833–13839. https://doi.org/10.1021/ja905467v

550 Hu, J., Chen, D., Li, N., Xu, Q., Li, H., He, J., Lu, J., 2018. Fabrication of graphitic-C_3N_4 quantum
551 dots/graphene-$InVO_4$ aerogel hybrids with enhanced photocatalytic NO removal under
552 visible-light irradiation. Appl. Catal. B Environ. 236, 45–52.
553 https://doi.org/10.1016/j.apcatb.2018.04.080

554 Huang, Y., Zhu, D., Zhang, Q., Zhang, Y., Cao, J., Shen, Z., Ho, W., Lee, S.C., 2018. Synthesis of a
555 $Bi_2O_2CO_3/ZnFe_2O_4$ heterojunction with enhanced photocatalytic activity for visible light
556 irradiation-induced NO removal. Appl. Catal. B Environ. 234, 70–78.
557 https://doi.org/10.1016/j.apcatb.2018.04.039

558 Huo, W., Xu, W., Cao, T., Guo, Z., Liu, X., Ge, G., Li, N., Lan, T., Yao, H.C., Zhang, Y., Dong, F.,
559 2019a. Carbonate doped Bi_2MoO_6 hierarchical nanostructure with enhanced
560 transformation of active radicals for efficient photocatalytic removal of NO. J. Colloid
561 Interface Sci. 557, 820–828. https://doi.org/10.1016/j.jcis.2019.09.089

562 Huo, W., Xu, W., Cao, T., Liu, X., Zhang, Y., Dong, F., 2019b. Carbonate-intercalated defective
563 bismuth tungstate for efficiently photocatalytic NO removal and promotion mechanism
564 study. Appl. Catal. B Environ. 254, 206–213. https://doi.org/10.1016/j.apcatb.2019.04.099

565 Kim, J.H., Han, J.H., Jung, Y.C., Kim, Y.A., 2019. Mussel adhesive protein-coated titanium oxide
566 nanoparticles for effective NO removal from versatile substrates. Chem. Eng. J. 378,
567 122164. https://doi.org/https://doi.org/10.1016/j.cej.2019.122164

568 Kim, S.Y., Cho, Y.J., Lee, A.R., Son, H., Han, W.S., Cho, D.W., Kang, S.O., 2017. Influence of π-
569 conjugation structural changes on intramolecular charge transfer and photoinduced
570 electron transfer in donor-π-acceptor dyads. Phys. Chem. Chem. Phys. 19, 426–435.
571 https://doi.org/10.1039/c6cp06566j

572 Kim, S., Fahel, J., Durand, P., Andre, E., Carteret, C., 2017. Ternary layered double hydroxides
573 (LDH) based on ZnAl substituted with Co, Cu for efficient photocatalysts design. Eur. J. Inorg.
574 Chem. 669–678. https://doi.org/10.1002/ejic.201601213

575 Leinen, M.B., Dede, D., Khan, M.U., Caglayan, M., Kocak, Y., Demir, H.V., Ozensoy, E., 2019. CdTe
576 Quantum Dot-Functionalized P25 Titania Composite with Enhanced Photocatalytic NO_2
577 Storage Selectivity under UV and Vis Irradiation. ACS Appl. Mater. Interfaces 11, 865–879.
578 https://doi.org/10.1021/acsami.8b18036

579 Lewis, R.J., 2012. Sax's Dangerous Properties of Industrial Materials, 5 Volume Set, 12th Edition,
580 Twelth. ed. Wiley & Sons, New Jersey.

581 Liao, J., Cui, W., Li, J., Sheng, J., Wang, H., Dong, X., Chen, P., Jiang, G., Wang, Z., Dong, F., 2020.
582 Nitrogen defect structure and NO+ intermediate promoted photocatalytic NO removal on
583 H_2 treated g-C_3N_4. Chem. Eng. J. 379. https://doi.org/10.1016/j.cej.2019.122282

584 Lv, X., Zhang, J., Dong, X., Pan, J., Zhang, W., Wang, W., Jiang, G., Dong, F., 2020. Layered double
585 hydroxide nanosheets as efficient photocatalysts for NO removal: Band structure
586 engineering and surface hydroxyl ions activation. Appl. Catal. B Environ. 277, 119200.
587 https://doi.org/https://doi.org/10.1016/j.apcatb.2020.119200

588 Mohapatra, L., Parida, K., 2016. A review on the recent progress, challenges and perspective of
589 layered double hydroxides as promising photocatalysts. J. Mater. Chem. A 4, 10744–10766.
590 https://doi.org/10.1039/C6TA01668E

591 Mullen, M.R., Dutta, P.K., 2016. Building Selectivity for NO Sensing in a NO_x Mixture with
592 Sonochemically Prepared CuO Structures. Chemosensors 4.
593 https://doi.org/10.3390/chemosensors4010001

594 Parida, K., Mohapatra, L., 2012. Recent progress in the development of carbonate-intercalated
595 Zn/Cr LDH as a novel photocatalyst for hydrogen evolution aimed at the utilization of solar
596 light. Dalt. Trans. 41, 1173–1178. https://doi.org/10.1039/C1DT10957J

597 Pastor, A., Balbuena, J., Cruz-Yusta, M., Pavlovic, I., Sanchez, L., 2019. ZnO on rice husk: A
598 sustainable photocatalyst for urban air purification. Chem. Eng. J. 368, 659–667.
599 https://doi.org/10.1016/j.cej.2019.03.012

600 Pastor, A., Rodriguez-Rivas, F., de Miguel, G., Cruz-Yusta, M., Martin, F., Pavlovic, I., Sanchez, L.,
601 2020. Effects of Fe^{3+} substitution on Zn-Al layered double hydroxides for enhanced NO
602 photochemical abatement. Chem. Eng. J. 387. https://doi.org/10.1016/j.cej.2020.124110

603 Perez, M.R., Crespo, I., Ulibarri, M.A., Barriga, C., Rives, V., Fernandez, J.M., 2012. Influence of
604 divalent metal on the decomposition products of hydrotalcite-like ternary systems M^{II}-Al-Cr
605 (M^{II} = Zn, Cd). Mater. Chem. Phys. 132, 375–386.
606 https://doi.org/10.1016/j.matchemphys.2011.11.040

607 Rives, V., 2001. Layered double hydroxides: present and future. Nova Publishers.

608 Rodriguez-Rivas, F., Pastor, A., Barriga, C., Cruz-Yusta, M., Sanchez, L., Pavlovic, I., 2018. Zn-Al
609 layered double hydroxides as efficient photocatalysts for NO_x abatement. Chem. Eng. J. 346,
610 151–158. https://doi.org/10.1016/j.cej.2018.04.022

611 Rodriguez-Rivas, F., Pastor, A., de Miguel, G., Cruz-Yusta, M., Pavlovic, I., Sanchez, L., 2020. Cr^{3+}
612 substituted Zn-Al layered double hydroxides as UV-Vis light photocatalysts for NO gas
613 removal from the urban environment. Sci. Total Environ. 706.

https://doi.org/10.1016/j.scitotenv.2019.136009

Shang, H., Li, M., Li, H., Huang, S., Mao, C., Ai, Z., Zhang, L., 2019. Oxygen Vacancies Promoted the Selective Photocatalytic Removal of NO with Blue TiO_2 via Simultaneous Molecular Oxygen Activation and Photogenerated Hole Annihilation. Environ. Sci. Technol. 53, 6444–6453. https://doi.org/10.1021/acs.est.8b07322

Shao, M., Han, J., Wei, M., Evans, D.G., Duan, X., 2011. The synthesis of hierarchical Zn-Ti layered double hydroxide for efficient visible-light photocatalysis. Chem. Eng. J. 168, 519–524. https://doi.org/10.1016/j.cej.2011.01.016

Shen, T., Shi, X., Guo, J., Li, J., Yuan, S., 2021. Photocatalytic removal of NO by light-driven Mn_3O_4/BiOCl heterojunction photocatalyst: Optimization and mechanism. Chem. Eng. J. 408, 128014. https://doi.org/https://doi.org/10.1016/j.cej.2020.128014

Tan, B., Zhang, X., Li, Y., Chen, H., Ye, X., Wang, Y., Ye, J., 2017. Anatase TiO_2 Mesocrystals: Green Synthesis, In Situ Conversion to Porous Single Crystals, and Self-Doping Ti^{3+} for Enhanced Visible Light Driven Photocatalytic Removal of NO. Chem. Eur. J. 23, 5478–5487. https://doi.org/10.1002/chem.201605294

Tang, J., Zou, Z., Ye, J., 2004. Efficient Photocatalytic Decomposition of Organic Contaminants over $CaBi_2O_4$ under Visible-Light Irradiation. Angew. Chemie Int. Ed. 43, 4463–4466. https://doi.org/10.1002/anie.200353594

Wang, C., Ma, B., Xu, S., Li, D., He, S., Zhao, Y., Han, J., Wei, M., Evans, D.G., Duan, X., 2017. Visible-light-driven overall water splitting with a largely-enhanced efficiency over a Cu_2O@ZnCr-layered double hydroxide photocatalyst. Nano Energy 32, 463–469. https://doi.org/https://doi.org/10.1016/j.nanoen.2017.01.010

Wang, H., Zhao, R., Hu, H., Fan, X., Zhang, D., Wang, D., 2020. 0D/2D Heterojunctions of Ti_3C_2 MXene QDs/SiC as an Efficient and Robust Photocatalyst for Boosting the Visible Photocatalytic NO Pollutant Removal Ability. ACS Appl. Mater. Interfaces 12, 40176–40185. https://doi.org/10.1021/acsami.0c01013

Wang, X.D., Summers, C.J., Wang, Z.L., 2004. Mesoporous Single-Crystal ZnO Nanowires Epitaxially Sheathed with Zn_2SiO_4. Adv. Mater. 16, 1215–1218. https://doi.org/10.1002/adma.200306505

Wu, H., Yuan, C., Chen, R., Wang, J., Dong, F., Li, J., Sun, Y., 2020. Mechanisms of Interfacial Charge Transfer and Photocatalytic NO Oxidation on BiOBr/SnO2 p–n Heterojunctions. ACS Appl. Mater. Interfaces 12, 43741–43749. https://doi.org/10.1021/acsami.0c12628

Xiang, X., Li, F., Huang, Z., 2014. Recent Advances in Layered Double Hydroxide-Based Materials as Versatile Photocatalysts. Rev. Adv. Sci. Eng. 3, 158–171. https://doi.org/10.1166/rase.2014.1060

Xiao, S., Pan, D., Liang, R., Dai, W., Zhang, Q., Zhang, G., Su, C., Li, H., Chen, W., 2018. Bimetal MOF derived mesocrystal $ZnCo_2O_4$ on rGO with High performance in visible-light photocatalytic NO oxidization. Appl. Catal. B Environ. 236, 304–313. https://doi.org/10.1016/j.apcatb.2018.05.033

653 Xu, S.M., Yan, H., Wei, M., 2017. Band Structure Engineering of Transition-Metal-Based Layered
654 Double Hydroxides toward Photocatalytic Oxygen Evolution from Water: A Theoretical–
655 Experimental Combination Study. J. Phys. Chem. C 121, 2683–2695.
656 https://doi.org/10.1021/acs.jpcc.6b10159

657 Yang, Q., Wang, S., Chen, F., Luo, K., Sun, J., Gong, C., Yao, F., Wang, X., Wu, J., Li, X., Wang, D.,
658 Zeng, G., 2017. Enhanced visible-light-driven photocatalytic removal of refractory pollutants
659 by Zn/Fe mixed metal oxide derived from layered double hydroxide. Catal. Commun. 99,
660 15–19. https://doi.org/10.1016/j.catcom.2017.05.010

661 Yang, Z., Wei, J., Zeng, G., Zhang, H., Tan, X., Ma, C., Li, X., Li, Z., Zhang, C., 2019. A review on
662 strategies to LDH-based materials to improve adsorption capacity and photoreduction
663 efficiency for CO_2. Coord. Chem. Rev. 386, 154–182.
664 https://doi.org/10.1016/j.ccr.2019.01.018

665

Highlights

- $Zn_{2-x}Cu_2Cr$ LHDs are effective UV-Vis light De-NO_X photocatalysts

- The Zn^{2+} by Cu^{2+} ion replacement increases the surface area and light absorption

- The Cu centres create new states in the valence band.

- The production of ROS species is favoured in doped samples.

Declaration of interests

☒ The authors declare that they have no known competing financial interests or personal relationships that could have appeared to influence the work reported in this paper.

☐The authors declare the following financial interests/personal relationships which may be considered as potential competing interests: